Adsorption and Desorption of Chiral Molecules on Gold Substrate in Magnetic Fields

by

Shangyu Qian

B. Sc. in Chemistry, Peking University, 2015

Submitted to the Graduate Faculty of the

Dietrich School of Arts and Sciences in partial fulfillment

of the requirements for the degree of

Master of Science

University of Pittsburgh

2020

UNIVERSITY OF PITTSBURGH

DIETRICH SCHOOL OF ARTS AND SCIENCES

This thesis was presented

by

Shangyu Qian

It was defended on

April 8, 2020

and approved by

Shigeru Amemiya, Professor, Department of Chemistry

Steve Weber, Professor, Department of Chemistry

Thesis Advisor: David Waldeck, Professor, Department of Chemistry

Adsorption and Desorption of Chiral Molecules on Gold Substrate in Magnetic Fields

Shangyu Qian, MS

University of Pittsburgh, 2020

The chiral-induced spin selectivity (CISS) effect refers to the fact that when electrons transit through a chiral molecule (or structure), the chiral potential leads to an effective magnetic field in the rest frame of the electron that acts on the electron spin, providing a preference for the transmission of one electron spin orientation over the other. Because of the CISS effect, the interaction between a magnetized surface and a chiral molecule will depend on the enantiomer and on the magnetization direction of the magnetized substrate. This work aims to better understand the interaction between a ferromagnetic surface and chiral molecules and use the knowledge to establish a method of enantiomer separation. An electrochemical quartz crystal microbalance (EQCM) is used to study the electrochemical adsorption and desorption for different enantiomers of a chiral molecule, cysteine, onto ferromagnetic substrates under an external magnetic field, both thermodynamically and kinetically. The results show that the kinetics for adsorption and desorption of a chiral molecule depends on the magnetization direction of the surface.

Table of Contents

List of Tables

List of Figures

Acknowledgement

I would like to express the deepest appreciation to my research advisor, Professor David Waldeck, who has the tremendous wisdom and insight in chemistry research and a warm heart towards me. The knowledge I acquired within these years would be a treasure for my future life.

I would like to appreciate the suggestions and help by the committee members, Professor Shigeru Amemiya and Professor Steve Weber, in the completion of this thesis and my thesis defense.

I would like to thank the group members, Dr. Brian Bloom, Dr. Edward Beall, Jimeng Wei, Caleb Clever, Supriya Ghosh, Zheni Georgieva, Yiyang Lu, Ford Smith, Alexander Craig. The kind help from you build my confidence in challenging myself.

I also record my thanks to Professor Ron Naaman and his group from Weizmann Institute of Science. The collaboration with you provided me aspects to observe the unknown world from different angles.

I would like to express my appreciation to my wife, Yi Wang. Your encouragement and support throughout my completion of the thesis is the most power for me to pace on.

1   **Introduction**

1.1   **Chiral-Induced Spin Selectivity**

Chiral-induced spin selectivity (CISS) effect refers to the fact that when electrons transit through a chiral molecule (or structure), the chiral potential leads to an effective magnetic field in the rest frame of the electron that acts on the electron spin, providing a preference for the transmission of one electron spin orientation over the other[1-3]. It was first observed in 1999 that an asymmetric scattering of photoelectrons in spin existed in photoelectron transmission studies, where the photoelectrons ejected from an Au substrate transmitted through Langmuir-Blodgett (LB) films of L- or D-stearoyl lysine[1].
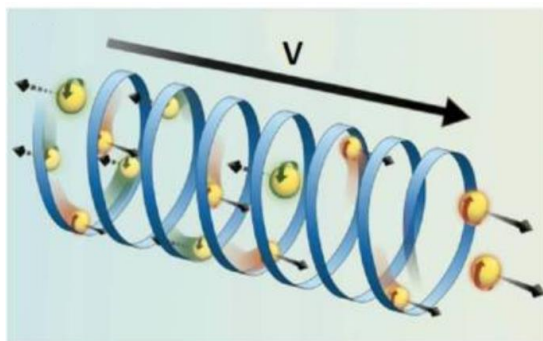
Figure 1-1 Schematic illustration of the CISS effect. When electrons with different spin states (marked with green and red arrows) move through a chiral molecule, the interaction of electron velocity and the chiral electric field will prefer electrons with one spin state to transmit over the other. This figure is taken from reference 4.

When an electron moves through a chiral molecule, the electrostatic potential of the molecule, which is also chiral, interacts with the electron. A schematic illustration of the CISS

effect is shown in Figure 1-1. The interaction of electron velocity and the chiral electric field of molecule generates an effective magnetic field $\vec{B}$:

$$\vec{B} = \frac{\vec{v}}{c^2} \times \vec{E}_{chiral}$$

in which $\vec{v}$ is the velocity of the electron, c is the speed of light, and $\vec{E}_{chiral}$ is the chiral potential of the molecule.

The early works on spin-specific applications were usually associated either with magnetic materials (for example, the giant magnetoresistance effect, or GMR)[4-5] or with materials that have very large spin-orbit coupling (SOC)[6-7]. The SOC that interacts with the electrons in these cases is referred to as Dresselhaus (bulk inversion asymmetry)[8] or Rashba (structural inversion asymmetry)[9] SOC term.

The term in the Hamiltonian for the SOC[10] is given by:

$$H_{SOC} = \lambda \vec{\sigma} \cdot (\vec{p} \times \vec{E}_{chiral})$$

in which $\lambda = \frac{e\hbar}{4m^2c^2}$, $\vec{p}$ is the electron momentum, m is the electron's mass, and $\vec{\sigma}$ are the Pauli matrices and represent the electron's spin state. It indicates that SOC is generated by the coupling of the linear momentum of the electron and its spin state.

If we consider the spin and the velocity direction as two kinds of parameters for the electron, we can define the electrons which moves through the chiral potential within the chiral molecule with 4 different momentum-spin states, which are denoted as in Figure 1-2 An energy scheme for the momentum-spin states, |momentum, spin>, of an electron moving within a helical electric field. The spin alignment flips with the handedness of the helix. For the electron moving in positive direction (+), the interaction with $\vec{E}_{chiral}$ splits the electrons with different spin, which are in states |+,+> and |+,->, with the energy gap of $2H_{SOC}$. In a left handed helix, state |+,+> is stabilized by

the spin-orbit energy, H_{SOC}, whereas |+,-> is destabilized by the same energy. In a right handed helix, however, state |+,+> is destabilized and |+,-> is stabilized by H_{SOC}. When the electron velocity direction is reversed (-), the stabilization related to spin has the reverse direction, which makes the state |+,+> degenerate with |-,->, and |+,-> degenerates with |-,+>.

Consider a case when an electron is backscattered in direction while retaining its spin state within the left-handed helical molecule, which changes its state from |+,+> to |-,+>. In order to change the state the electron must acquire more energy than $2\,H_{SOC}$ to populate the higher momentum-spin states. The fraction of the population, P_{bs}, that has energy exceeding the energy of the |-,+> state is given by possibility distribution

$$P_{bs} = \exp\left(-\frac{2H_{soc}}{kT}\right)$$

where k is the Boltzmann constant and T is the temperature in Kelvin. For an H_{SOC} value of ~100 cm^{-1} (12.4 meV) for small molecules[11], the P_{bs} value is around 0.38. But for an H_{SOC} value of 0.5 eV for a double-strand DNA (dsDNA) oligomer[12] at room temperature, the P_{bs} value reaches the order of 1.3×10^{-17}, which indicates the backscattering is unfavorable. This explains the effect of spin-filtering of CISS, which shows the preference of electron movement within a chiral molecule when the spin and the handedness is given.
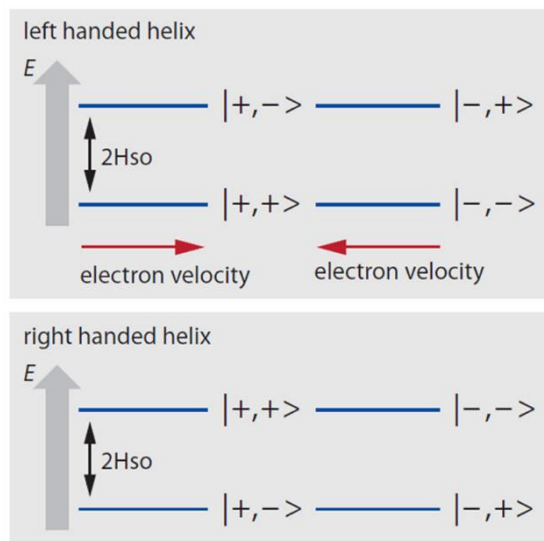
Figure 1-2 An energy scheme for the momentum-spin states, |momentum, spin>, of an electron moving within a helical electric field. The spin alignment flips with the handedness of the helix. This figure is taken from reference 3.

1.2   Methods of Measuring Spin Selectivity

We define the spin polarization or spin selectivity (S) as

$$S = \frac{N_+ - N_-}{N_+ + N_-}$$

where N_+ and N_- are the spin populations in the process between spins oriented parallel and antiparallel within the experiment. This asymmetry parameter can be used in many different experiments, such as the spin polarized photoelectron yield[13], Hall voltage in spin Hall devices[12, 14], and current in spin-dependent electrochemistry[15]. Several methods have so far been applied in experiments to measure spin-selective transport through molecules and the observations have led to the discovery of the CISS effects. There are mainly aspects of measurement: photoelectron transmission, electron transport, and electron transfer.

The first discovery of the CISS effect was obtained by photoelectron transmission experiments on LB films of chiral molecules[1], and the spin dependent transmission was inferred from photoelectron quantum yields. In later works, a Mott polarimeter was introduced[13], which could directly measure the spin polarization of photoelectrons by their angular distribution. For a bare Au (111) surface, the spin polarization was controlled by the polarization of incident light. The spin polarization of photoelectrons changes from -22% for the cw circularly polarized light, to 0% for linear polarized light, and to +22% for the ccw. When a SAM of a 50-base pairs (bp) double-stranded DNA (dsDNA) was coated onto the Au substrate, however, the spin polarization is nearly independent of the incident light polarization: -35% for cw, -31% for linear, and -29% for ccw. The results are shown in Figure 1-3.
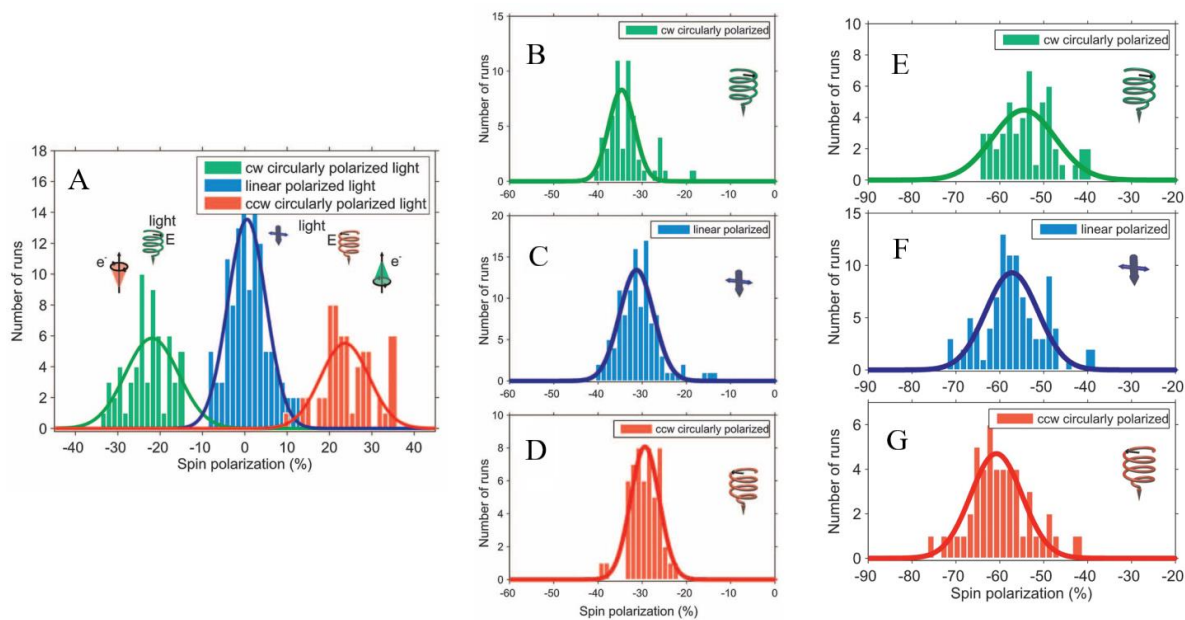
Figure 1-3 The spin polarization measurement for photoelectrons ejected from (A) bare Au (111) surface, (B) ~ (D) 50-bp dsDNA/Au(111), and (E) ~ (G) 78-bp dsDNA/Au(111). The 78-bp dsDNA showed even larger spin polarization values, which indicates that the CISS effect is related to the properties of chiral molecules. This figure is taken from reference 13.

Electron transport measurements, for example magnetoresistance[16], conductance[12], and Hall measurements[14], involve the movement of electrons between two electrodes. The CISS effect is investigated and monitored in these cases by transporting the electrons through a chiral molecule layer. Ravi *et al.* reported the change in magnetoresistance and spin-filtering efficiency measurement of a sandwich-like nanostructure.[16] In this study, the device comprises a nonmagnetic film deposited between two ferromagnetic (FM) electrodes, and the electric current flowing through the device is measured versus the external magnetic field. A monolayer of DNA was deposited between two FeCo films to make a FM/DNA/FM based junction, which makes the change in current after applying a magnetic field different from that measured with a device without the DNA monolayer. The spin-filtering efficiency was calculated to be 30%, which is half of the value by pure gold surface coated with DNA. Xie *et al.* performed a similar experiment by using conductive probe atomic force microscopy (CP-AFM) and observed magnetic field dependent changes in the conductance of dsDNA molecules[12].

The CISS effect has also been reported in electrochemical junction experiments[15, 17]. Similar to the electron transport studies, a FM working electrode is used and a monolayer of chiral molecules is adsorbed on it. The redox couple for electrochemical reaction can be in the electrolyte solution or can be attached to the chiral molecule monolayer. Similar to the CP-AFM study above, the existence of an external magnetic field will split the valence band of the FM electrode and make the transferring electron spin-specific, then filtered by the chiral monolayer. The spin-filter will cause a difference in faradaic current when the magnetic field direction is pointing UP (j_+) or DOWN (j_-) in direction, and the spin polarizationcan can be calculated from the asymmetry in the current.

1.3 SAM of Thiols on Gold Substrate

Self-assembled monolayer (SAM) of thiols, or mercapto group containing organic molecules on gold have been widely applied in nanoscience studies[18].

A thiol molecule consists of three parts:

1. The surface headgroup ($-SH$, or the deprotonated form, $-S^-$), which forms a strong covalent bond with the gold substrate;

2. The organic chain, which stabilizes the monolayer through van der Waals interactions;

3. The terminal group, which affects the physical and chemical properties significantly, whether highly hydrophobic ($-CH_3$, $-CF_3$, etc.) or hydrophilic and with good binding properties towards metal ions or biomolecules ($-COOH$, $-NH_2$, $-OH$, etc.).

A SAM of thiols is usually grown onto a gold surface by immersing the gold substrate in a thiol-containing solution[19-21]. Voltammetry of the electrochemical reductive desorption of the SAM in a basic aqueous solution was first reported by Porter *et al.*[22] and can be used to diagnose and engineer SAMs. The half reduction reaction is

$$M\text{-}SR + e^- = M + RS^-$$
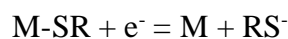
The reduction gives rise to a sharp cathodic peak, and the peak position is affected by the length of hydrocarbon group of thiols[19], pH value of the solution[23], and the face index of gold substrate[24], etc.

1.4   Langmuir Adsorption Isotherm Model

The Langmuir adsorption model is commonly applied to explain the adsorption behavior of molecules on a solid surface. It was first presented by Irving Langmuir in 1916[25], where he hypothesized that a given surface has a certain number of equivalent sites to which a species can "stick", either physically or chemically, as shown in Figure 1-4[26].

The basic assumptions of this model are as following[27]:

1.   The surface containing the adsorbing sites is a perfectly flat, homogeneous plane.

2.   The surface of the adsorbent is in contact with a phase containing an adsorbate which is strongly attracted to the surface.

3.   The surface has a specific number of sites where the solute molecules can be adsorbed, and all sites are equivalent.

4.   The adsorption involves the attachment of only one layer of molecules to the surface, i. e. monolayer adsorption.

5.   There are no interactions between adsorbate molecules on adjacent sites.
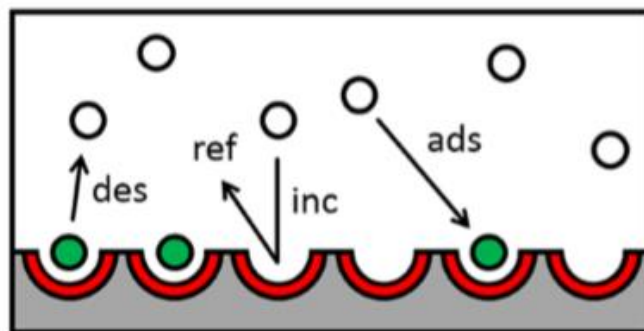
Figure 1-4 A schematic showing the adsorption model. All adsorbing sites (red semicircles) are equivalent and can be occupied (green dots) by only one molecule adsorbates(white dots). The adsorption involves 4 different processes: incidence (inc), reflection (ref), adsorption (ads) and desorption (des). Treating these processes with the basic approximations leads to the isotherm equation. This figure is taken from reference 26.

Assume that the adsorption is a reversible chemical reaction

$$A + S \leftrightarrow AS$$

where A represents the adsorbate, S represents unoccupied adsorbing sites on the adsorbent, and AS represents occupied sites. We have the equilibrium constant to be

$$K_{ADS} = \frac{[AS]}{[A][S]}$$

Note here that $[A]$ is the concentration of adsorbate A in the solution.

Define Y as the amount of adsorption, which can be mass of adsorbate, mass density (mass per unit mass adsorbent), moles of adsorbate per unit area adsorbent, etc., and Y_{Max} as the maximum adsorption amount possible for the adsorbent. And the general form of adsorption isotherm can be expressed as:

$$Y = \frac{Y_{Max}K_{ADS}C}{1 + K_{ADS}C}$$

Or the rearranged linear form:

$$\frac{C}{Y} = \frac{1}{K_{ADS}Y_{Max}} + \frac{C}{Y_{Max}}$$

where C equals $[A]$, the plot of $\frac{C}{Y}$ vs C is a linear plot, and the maximum adsorption amount and the adsorption equilibrium constant K_{ADS} can be calculated by the slope and intercept value of the linear plot. From the K_{ADS}, the Gibbs free energy of the adsorption can be calculated

$$K_{ADS} = \frac{1}{c_{solvent}} \exp\left(\frac{-\Delta G_{ADS}}{RT}\right)$$

where $c_{solvent}$ is the concentration of the solvent (which is usually close to the concentration of pure solvent for low concentration solutions), and thus gain information about the strength of interaction between adsorbates and adsorbents.

9

A general form of Langmuir isotherm is presented in Figure 1-5, where the amount of adsorption Y is presented as mass change $|\Delta m|$ of protein adsorption on a Pt substrate. A regular Langmuir isotherm of $|\Delta m|$ versus [Protein] is plotted, which shows a plateau of $|\Delta m|$ that indicates the maximum adsorption. A linearized isotherm [Protein] / $|\Delta m|$ versus [Protein] is plotted in the inner panel.
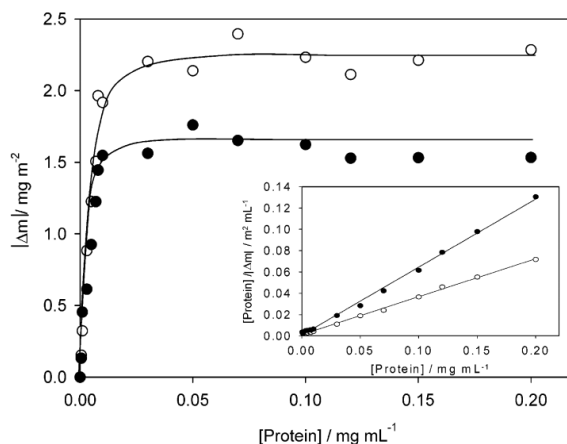
Figure 1-5 A general form of the Langmuir isotherm plot, where the two kinds of dots are the experimental data of two different kinds of protein adsorption mass change $|\Delta m|$, and the solid line is the fitted isotherm. The inner panel shows the linearized isotherm plot. This figure is taken fro reference 26.

1.5   Electrochemical Quartz Crystal Microbalance

A quartz crystal microbalance (QCM) (also known as quartz crystal nanobalance (QCN)) measures a mass change by measuring the change in frequency of a quartz crystal resonator[28]. A QCM applies the inverse piezoelectric effect, where an alternating potential is applied across the quartz crystal disk to generate transverse acoustic wave across the thickness of the disk, see Figure 1-6.

The fundamental frequency of the wave can be calculated by

$$f_0 = \frac{v_{tr}}{2t_Q}$$

where v_{tr} is the transverse velocity (the velocity of sound), and t_Q is the thickness of the quartz resonator. If the quartz crystal is covered with a rigid overlayer, for example L-cysteine SAM on a gold substrate, the thickness of the overlayer is added to the overall t_Q, which will reduce the frequency of the wave. The dependence is explained by the Sauerbrey equation:[29]

$$\Delta f = \frac{-2f_0^2}{A\sqrt{\mu\rho}}\Delta m,$$

where f_0 is the resonant frequency of the fundamental mode of quartz resonator, Δf is the normalized frequency change, Δm is the mass change, A is the piezoelectrically active quartz crystal area, ρ is the density of quartz (2.648 g·cm^{-3}), and μ is the shear modulus of quartz crystal (for the AT-cut crystal that is applied in QCM, μ = 2.947×10^{11} g·cm^{-1}·s^{-2}). For a quartz crystal resonator in QCM, we can calculate the mass change on the quartz crystal directly from the normalized frequency change.
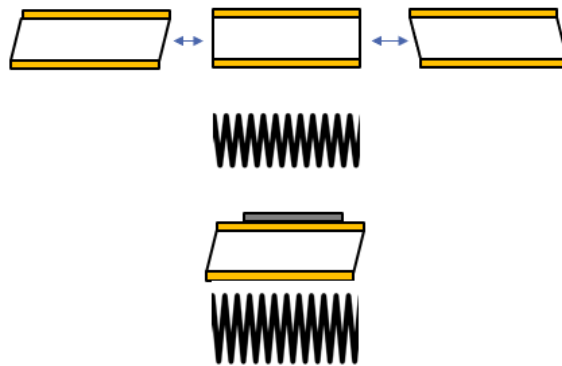
Figure 1-6 Schematic illustration of the mechanism of QCM. A QCM applies the inverse piezoelectric effect, where an alternating potential is applied across the quartz crystal disk to generate transverse acoustic wave across the thickness of the disk and cause a vibration. If the quartz crystal is covered with a rigid overlayer, for example L-cysteine SAM, the SAM is treated as an extention of the crystal and the the thickness of the overlayer is added to the overall thickness t_Q, which will reduce the frequency of the wave.

An electrochemical quartz crystal microbalance (EQCM) is a device in which QCM is combined with a potentiostat or a galvanostat. An EQCM allows for the determination of mass deposited at the electrode surface during an electrochemical reaction, or its ratio to the total charge passed through the electrode (current efficiency). A typical structure of an EQCM instrument is shown in Figure 1-7. The quartz resonator works as the working electrode in the EQCM cell, where the electrochemical reaction occurs on the gold working area (whose area is the A in the Sauerbrey equation above), and the frequency change of the quartz crystal is recorded at the same time as the electrochemical measurement runs.
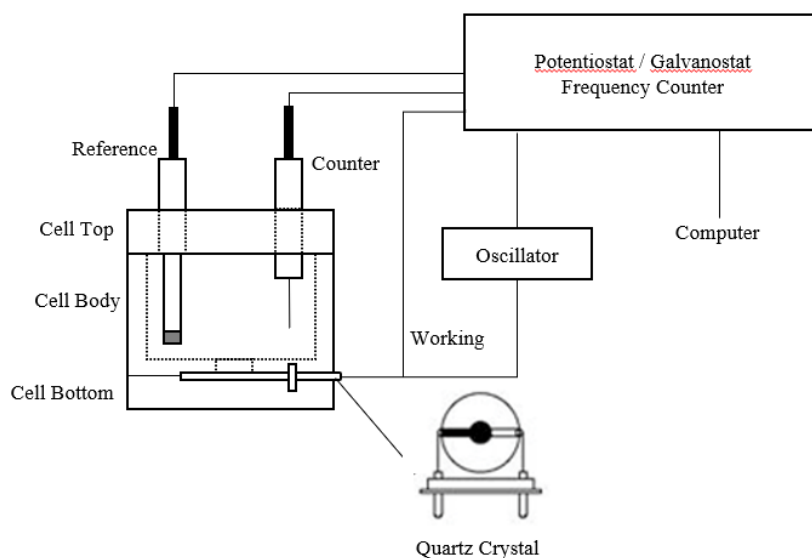
Figure 1-7 A typical schematic structure of an EQCM device.

1.6   Current Status of Enantiomer Separation

Producing pure enantiomers of chiral molecules is of great interest to the pharmaceutical industry since it is well known that for many drug compounds, one enantiomer will work with physiological effect, while the other often has no effect or is even harmful to human[30-31]. Techniques to produce pure enantiomers can be divided into mainly two approaches: (1) synthetic, to introduce asymmetric conditions which will cause the synthesis to preferentially produce one enantiomer over the other; (2) post synthetic, to separate the racemic mixtures of the two enantiomers. The latter approach is also called enantiomer separation or chiral resolution[32]. Two most promising enantiomer separation methods are crystallization and chromatography.

The first experiment using direct crystallization to separate enantiomers was done by Pasteur in 1848[33]. Since then, crystallization processes have been developed extensively for enantioseparation purposes. Crystallization methods include classical crystallization, where the racemic mixture is converted by an enantiomerically pure resolving agent to two diastereomeric salts with different solubilities[34]; preferential crystallization of conglomerates, where some kinds of chiral compounds (about 5 ~ 10% of all chiral compounds) will crystallize into enantiomerically pure crystals without a chiral agent[33-34]; optically active solvents, which can be chiral solvents or achiral solvents with a pure enantiomer as solute and will cause a difference in solubilities for the two enantiomers to be separated[35]. Crystallization bears the advantage of being simple and cost-efficient, comparing to other separation methods, while it is quite empirical for separation since the chiral agent or solvent matches the separation condition for only a few kinds of enantiomers.

Application of resolving agents similar as above into the stationary phase in chromatography, which makes the stationary phase chiral, makes chromatography a powerful enantiomer separation method[36]. Despite the good efficiency in separation and abilities to adjust

13

both the mobile phase and the stationary phase, the cost in both the instrument and amount of mobile phase (especially when using liquids) is quite considerable.

It was recently found that adsorption of chiral peptides on a magnetized ferromagnetic (FM) substrate depends on the chirality of peptide and the direction of magnetic dipole[37], as shown in Figure 1-8. An L- or D-polyalanine-based oligopeptide was exposed to a FM substrate (silicon with 1.8 nm of Co coated with 5 nm of Au) for 2s, and a clear difference in adsorption density was observed when the applied magnetic field was pointing UP or DOWN.
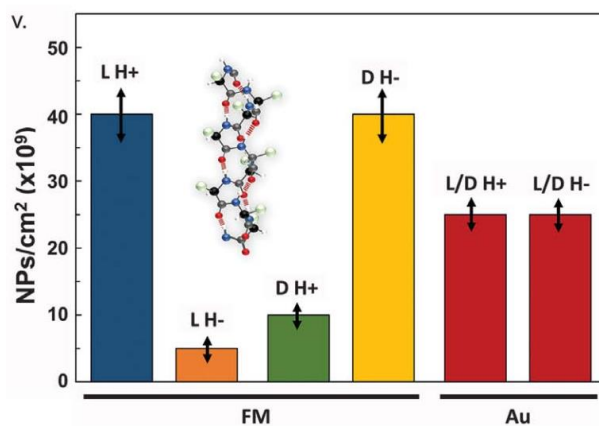
Figure 1-8 The adsorption density of L- or D-oligopeptide on FM layer with the magnet pointing UP (H+) or DOWN (H-). For comparation, the experiment was repeated by an Au substrate, which showed no difference in adsorption when the enantiomer or magnetic field direction was changed. The figure is taken from reference 35.

It was pointed out that because of CISS effect, the charge redistribution within a chiral molecule is accompanied by spin polarization, and the spin alignment at each electric pole depends on the specific enantiomer[38]. This makes the chiral molecule act as a molecular "magnet", and the interaction between a magnetized surface and a chiral molecule will thus depend on the enantiomer and on the magnetization direction of FM, as shown in Figure 1-9. Note here the interaction is controlled by electron spin orientations in the overlapping electron clouds, not by the magnetic

14

field. This enantioselective interaction between chiral molecules and FM substrates provides an approach to separate enantiomers with magnetic surfaces. Since the interaction depends on the charge polarization of the molecule (accompanied by spin polarization), which is general in chiral molecules, this separation method is thought to be applied to all chiral molecules.
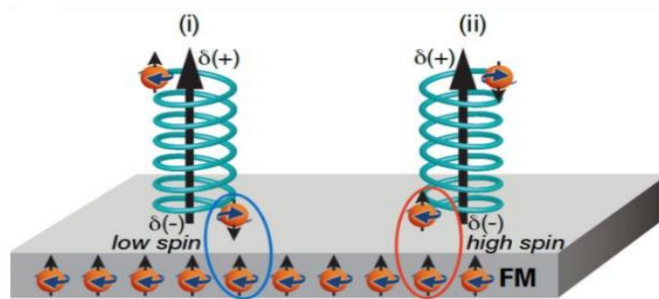
Figure 1-9 A scheme which illustrates spin effects on the interaction of a chiral molecule with a surface. The electrical polarization of the molecule is accompanied by a spin polarization. The spin alignment at each electric pole depends on the specific enantiomer. Therefore, the interaction between the magnetized surface and a given enantiomer follows either a high spin (i) or a low spin (ii) potential, depending on the direction of magnetization of the substrate. The figure is taken from reference 35.

1.7   This Work

This work aims to better understand the interaction between an FM surface and chiral molecules and use the knowledge to establish a method of enantiomer separation. As proposed, exposing one pole of a magnet to a racemic mixture should result in selective adsorption of one enantiomer over the other because of the interaction strength difference, and *vice versa*. Since CISS applies to all kinds of chiral molecules, the magnetic separation method can be general. Moreover, there is no demand for specific solvent or stationary phase, as is typically the case in chromatography, which could make the magnetic separation cost efficient.

An EQCM will be used to monitor the mass change during an electrochemical process. The electrochemical adsorption of different chiral molecules (with different enantiomers) will be performed in an EQCM cell, and the interaction between the chiral molecules and a FM quartz crystal (with a layer of Ni coated by a layer of Au) will be studied under an external magnetic field. Both thermodynamic (mass change at equilibrium vs concentration of adsorbate, and isotherm) and kinetic (mass change vs time, chronoamperometry) approaches will be applied, and the spin polarization in these cases will be calculated and compared.

2 Experimental

2.1 Electrochemistry and Isotherm for Adsorption of Cysteine on Au/Ni Electrode

An 7.9995 MHz quartz crystal (CH Instruments) was applied in an EQCM cell with a model 430A potentiostat from CH Instruments (the diagram of the full device is shown before in Figure 1-7). The surface area of the crystal is 0.205 cm^2 and is coated with polycrystalline gold as working electrode area. Prior to experiments the electrodes were cleaned by electrochemical treatment (- 1 V ~ + 1 V versus saturated Ag/AgCl for 50 cycles in 1 M H_2SO_4 for the first time use of quartz crystal, and − 1 V versus Ag/AgCl in potassium phosphate buffer for 1h before and after every use of the quartz crystal). To ensure the quartz crystal was functioning normally, an underpotential deposition (UPD) experiment of lead was performed using a 5 mM of $Pb(ClO_4)_2$, 10 mM of $HClO_4$ and 0.1M of $KClO_4$ solution[39]. Cyclic voltammograns (- 0.6 V ~ 0 V versus saturated Ag/AgCl) with QCM was measured in EQCM cell for lead deposition and it gave cathodic peak with the frequency decrease (adsorption of lead) at -0.52 V and anodic peak with frequency increase (desorption of lead) at -0.31 V. The frequency change of the crystal showed the EQCM with the quartz crystal functioned normally. L-cysteine (L-cys, purchased from Spectrum) or D-cysteine (D-cys, purchased from Sigma-Aldrich) solutions in 0.1 M pH =11.00 potassium phosphate buffer with several different concentrations were made, degassed by N_2 for 15 mins and 2 mL of those solutions were added to the EQCM cell, respectively. Cyclic voltammograms (CVs) were recorded (condition: - 1.1 V ~ - 0.4 V versus saturated Ag/AgCl, scan rate = 25 mV/s), as well as the frequency response of the quartz crystal. The frequency change (Δf) corresponding to the oxidative adsorption of cysteine on a gold substrate was calculated to mass

change (Δm) according to the Sauerbrey equation by a factor of - 1.4 ng / Hz. A typical result for CV with EQCM studies is shown in Figure 2-1. A cathodic peak at ~ -0.8V vs Ag/AgCl in voltammogram corresponding with frequency increase shows the reductive desorption of L-cys, whereas a wide anodic peak corresponding with frequency decrease shows the oxidative adsorption of L-cys. By plotting Δm versus c and fitting to a Langmuir – Freundlich isotherm model or plotting c/Δm versus c for a linear isotherm, Gibbs free energy (ΔG) of L-cys adsorption was calculated.
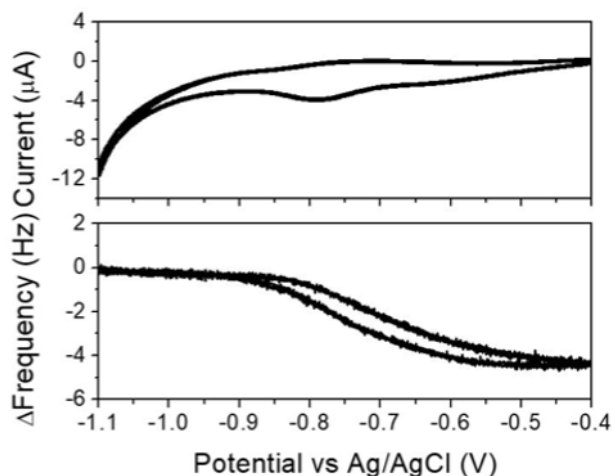
Figure 2-1 A representative cyclic voltammogram (top) and corresponding change in frequency (bottom) of the quartz crystal in the presence of L-cys. A cathodic peak at ~ -0.8V vs Ag/AgCl in voltammogram corresponding with frequency increase shows the reductive desorption of L-cys, whereas a wide anodic peak corresponding with frequency decrease shows the oxidative adsorption of L-cys.

To study the Gibbs free energy of adsorption, ΔG, under magnetization, a magnetic 7.9995 MHz quartz crystal (CH Instruments, custom) with a 100nm ferromagnetic nickel layer between gold layer and quartz was used for the EQCM cell. In order to prevent nickel oxidation under high pH environments, a 0.1M pH = 8.00 potassium phosphate buffer was applied for L-cys solution

instead. A neodymium magnet was applied underneath the cell with a 0.7 cm distance to the quartz crystal, which makes the magnetic field strength at the position of quartz crystal to be ~300 mT. The isotherm studies above were repeated with the north pole of the magnet pointing UP or DOWN and the ΔG of adsorption was compared for the two magnetic field directions. A schematic of our experiment design is shown in Figure 2-2.
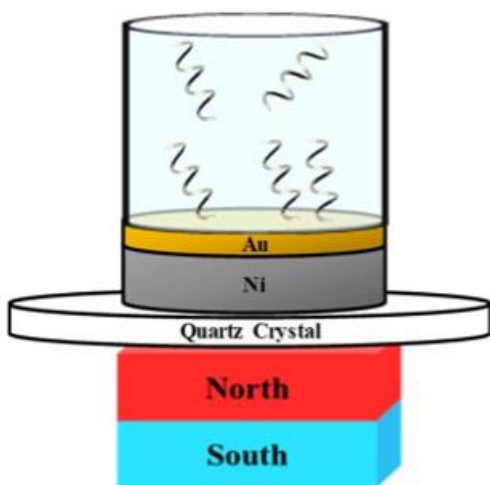
Figure 2-2 The experimental design. We applied a custom quartz crystal in EQCM cell with a 100 nm ferromagnetic nickel layer between ~10 nm gold layer and quartz. The magnet is applied underneath the cell and provides a magnetic field across the crystal.

2.2   Chronoamperometry Studies for Adsorption/Desorption of Cysteine on Au Electrode

Kinetics of the electrochemical adsorption and desorption of cysteine and the influence of magnetization on the kinetic behaviors were studied. CV with QCM was recorded for the same L-cys solution under the same conditions as above to find out at what potential adsorption and desorption occurs. Chronoamperometry studies were applied to further understand the kinetics of

the adsorption and desorption processes. The initial potential step was at a high potential ($\sim$-0.5 V) for oxidative adsorption and then stepped to a low potential ($\sim$-0.8 V) for reductive desorption. Chronoamperometry studies were done with custom magnetic quartz crystals, and frequency changes of crystals were recorded by QCM. The measurements were repeated with different L-cys or D-cys concentrations under magnetization (north pole pointing UP and DOWN). A typical result of chronoamperometry is shown in Figure 2-3, which showed that a change in frequency occurs upon jumping the potential corresponding to the adsorption and desorption of cysteine from the surface.

By assuming both the adsorption and desorption of cysteine is a 1st order reaction and fitting the frequency versus time data (or in fact, mass versus time data) in each step to a 1st order rate law, the rate constants of the adsorption and desorption were calculated. By comparing the rate constants under North magnetization and South magnetization, k_N and k_S, we calculated spin polarization by:

$$P = \frac{k_N - k_S}{k_N + k_S}$$

The chronoamperometry experiments were performed with 300+ steps (150+ cycles of adsorption and desorption) and a histogram of calculated rate constants was plotted. The influence of the cysteine concentration, step width, and solution pH on the spin polarization were studied.
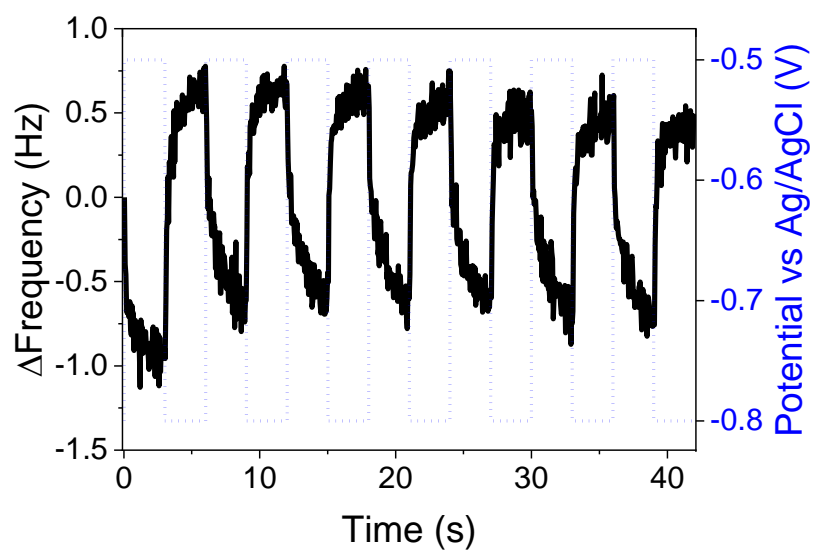
Figure 2-3 Chronoamperometry studies of cysteine solutions which showed that a change in frequency (black) occurs upon jumping the potential (blue) between -0.5 V and -0.8 V corresponding to the adsorption and desorption of cysteine from the surface.

3   Results and Discussion

3.1   Isotherm Study of Cysteine Oxidative Adsorption under Magnetic Fields

3.1.1 Characterization of Cysteine SAM Grown on Gold Surface

The electrochemical L-cys SAM growth on a gold substrate was achieved by oxidative adsorption. Under an applied voltage, an alkanethiol molecule electrochemically adsorbs on a gold electrode surface with the following half-reaction equation:

$$M + RSH = M(I)\text{-}SR + e^- + H^+$$

and it can be desorbed by reversing the voltage. The desorption of the alkanethiol molecule half-reaction is:

$$M\text{-}SR + e^- = M + RS^-$$
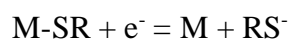
The adsorption gives an oxidative peak potential at -0.6 V ~ -0.8 V vs a saturated Ag/AgCl reference electrode, and the desorption gives a reductive peak potential at -0.8 V~-1.1 V vs Ag/AgCl, depending on the structure of thiol molecule[19]. Ellipsometry was used to measure the thickness of the SAM after oxidative adsorption onto the gold surface. Results are shown in Table 3-1.

Table 3-1 Ellipsometry results for L-cys SAM thickness measurements

Sample	Analyzer / °		Polarizer / °		Thickness / Å
	A1	A2	P1	P2	
Blank (Bare gold substrate)	43.5	136.0	80.4	170.6	-

Sample 1	Trial 1	43.5	136.1	80.5	171.1	6.11
	Trial 2	43.4	135.9	80.5	170.9	4.06
	Trial 3	43.0	135.8	80.4	171.1	5.07
Sample 2	Trial 1	42.8	135.9	80.2	171.4	6.07
	Trial 2	43.1	135.9	80.3	171.2	5.07
	Trial 3	43.3	135.6	80.4	171.2	6.13

The measured thickness of the SAM varies between 4 ~ 6 Å, whereas the length of L-cysteine is 7.1 Å[40]. The difference here is possibly because the gold substrate is not fully covered by L-cys or the L-cys adsorbed on gold is tilted.

A reductive desorption study on the L-cys SAM was performed. The gold substrate with L-cys SAM was used as the working electrode for a cyclic voltammetry (the potential window was -1.05 V ~ -0.2 V versus saturated Ag/AgCl, v = 25 mV/s) study in 0.5 M KOH aqueous solution. The voltammogram is shown as Figure 3-1. A cathodic peak occurs at -0.716 V versus saturated Ag/AgCl, whereas the literature data is -0.673 V versus saturated Ag/AgCl[24]. The cathodic peak disappears after the second scan, showing that cysteine has been stripped off after the first scan and is not able to be re-adsorbed due to the low concentration in solution.
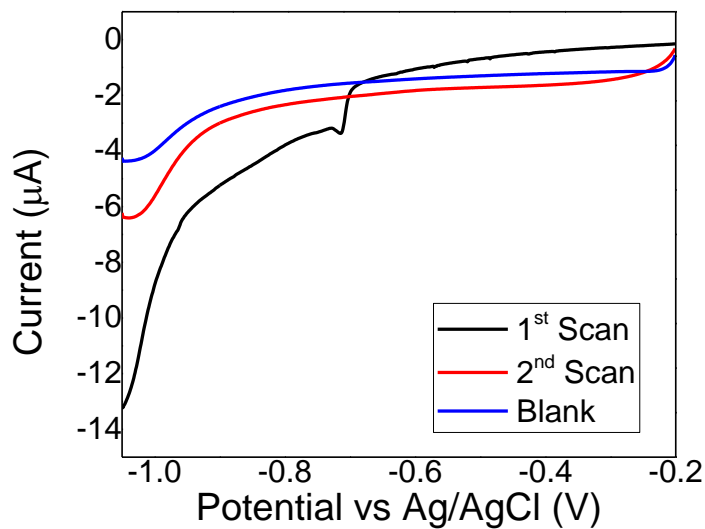
Figure 3-1 Voltammogram for L-cys reductive desorption. 0.5M KOH solution was used for blank comparison.

3.1.2 Adsorption/Desorption of L-cys, and Isotherm Results

When the cyclic voltammetry was run in a L-cys containing solution, the L-cys would be able to be oxidatively adsorbed on to and reductively desorbed off the surface. After ~30 scans the system was equilibrated and the adsorption and desorption reached to an equivalence, as shown in Figure 3-2.
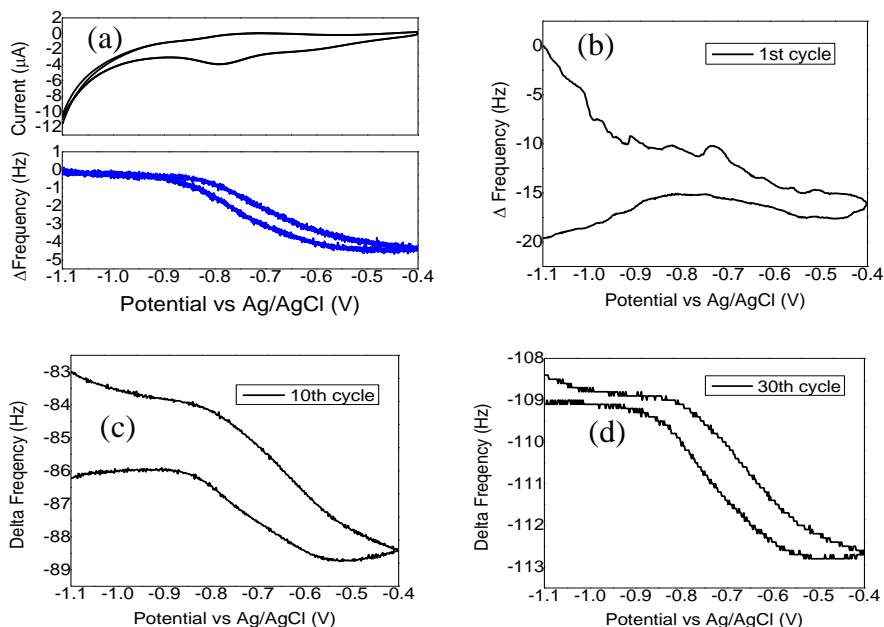
Figure 3-2 (a) Cyclic voltammogram and frequency change of L-cys oxidative adsorption and reductive desorption. (b) ~ (d) The equilibration of frequency change with scan numbers. Conditions: 0.2 mg/mL L-cys solution, -1.1 V ~ -0.4 V versus saturated Ag/AgCl, $v = 25$ mV/s.

The frequency change matched well with the cathodic and anodic peaks of the redox reaction. When the reduction reaction occurred, the frequency of the crystal was increasing which corresponded with mass decreasing. This was a clear sign of reductive desorption of cysteine. On the other hand, oxidation corresponded with mass increasing, which indicated an oxidative adsorption. The density of molecule coverage was calculated to be 1.3×10^{14} molecules/cm^{-2}. The literature value is 1.8×10^{14} cm^{-2} [21].

It needs to be pointed out that the pH selection 8 is not ideal for cysteine. Given the pK$_a$ values of cysteine: 1.71 (-COOH), 8.33 (-NH$_3^+$), 10.78 (-SH)[41], at pH=8 there is a major portion of cysteine existing in zwitterion form, which will cause the charge environment of the cysteine SAM to be beneficial for a electrostatic interaction between zwitterions, and even attachment of another layer, i.e. the formation of double or even multilayers of cysteine. In experiments,

25

adsorption of cysteine amount changes with measurement on different days but on the same crystals and with same experimental conditions. On the other hand, if the pH environment is basic enough, cysteine is more likely to dimerize and form cystine, which will decrease the amount of adsorption. Figure 3-3 shows a distribution of the mass change measured on the same quartz crystal for a 2 µg/mL L-cys solution adsorption under different pH environment. The adsorption mass change with pH values followed the conclusions above. At pH 10 we have a medium amount of adsorption, whereas at pH 8 we get a larger amount because of zwitterion effect and at pH > 11 we have a smaller amount caused by partial dimerization.
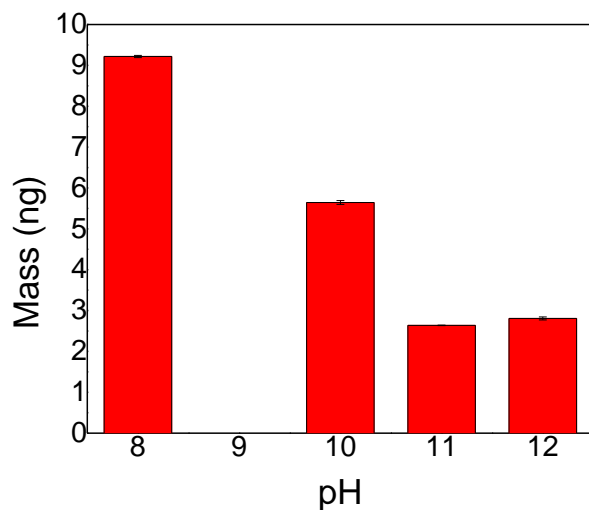
Figure 3-3 Mass change measured on the same quartz crystal for a 2 µg/mL L-cys solution adsorption under different pH environment.

To better understand the interaction between the L-cys and gold surface, the system was applied to a Langmuir adsorption model, as shown in Figure 3-4. It is calculated that the Gibbs free energy for L-cys adsorption is -34.2 ± 1.0 kJ/mol, which agrees well with the literature value as -34.8 kJ/mol[42]. The pH=8 data was used here for calculation.
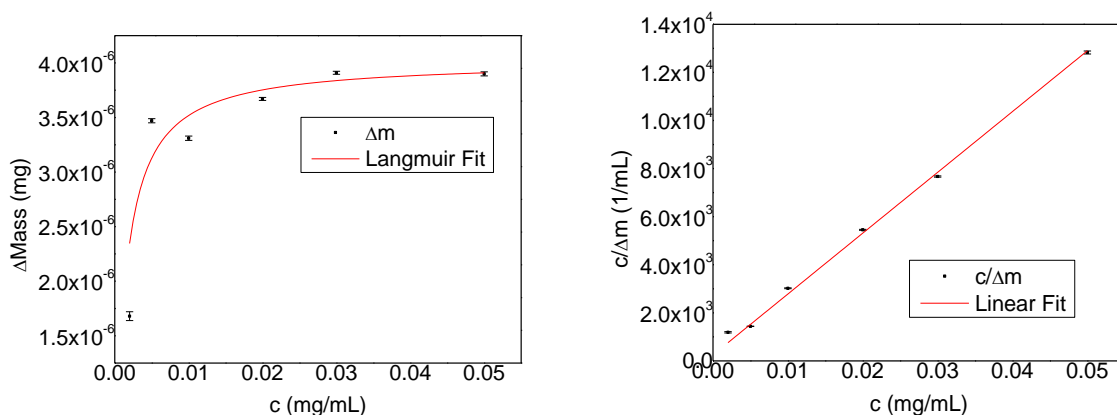
Figure 3-4 Langmuir isotherm (left) and linear isotherm (right) of L-cys adsorption.

3.1.3 Isotherm Results under Magnetic Fields

The isotherm study and ΔG_{ADS} study was repeated with the magnetic quartz crystal and under a magnetic field for multiple times. The results show some variation in the interaction strength between L-cys and gold substrate under different magnetic field directions, but without a trend, as shown in Table 3-2 The isotherm calculation results for L-cys adsorption under magnetic field with different directions. The definition of magnetization directions in the table is shown in Figure 3-5 The direction of magnetization as Parallel (left), North/N (mid), and South/S (right).

Table 3-2 The isotherm calculation results for L-cys adsorption under magnetic field with different directions

Magnetization Direction	$|\Delta m_{max}|$ / ng	Coverage / cm^{-2}	ΔG_{ADS} / kJ mol^{-1}	Error in ΔG_{ADS}[*]
No Magnetization	3.95	9.58×10^{13}	-34.2	1.0
#1 S	6.67	1.61×10^{14}	-31.9	2.4

#1 N	4.29	1.04×10^{14}	-35.3	2.1
#2 S	2.58	6.23×10^{13}	-34.6	1.5
#2 N	4.08	9.85×10^{13}	-33.8	0.6
#3 Parallel	5.19	1.26×10^{14}	-31.1	1.1
#3 S	5.47	1.33×10^{14}	-32.7	1.2
#3 N	3.62	8.78×10^{13}	-32.9	0.8
#4 Parallel	5.14	1.25×10^{14}	-31.4	1.0
#4 S	4.62	1.12×10^{14}	-32.1	1.0
#4 N	4.40	1.07×10^{14}	-32.9	1.1
#5 Parallel	2.56	6.21×10^{13}	-35.5	1.2
#5 S	2.60	6.31×10^{13}	-34.6	1.3
#5 N	2.89	7.01×10^{13}	-34.1	0.9

the runs with same number were done under same experimental conditions with the same quartz crystal, but under different magnetization.

* the error in ΔG_{ADS} was propagated from the error in fitting of isotherms.
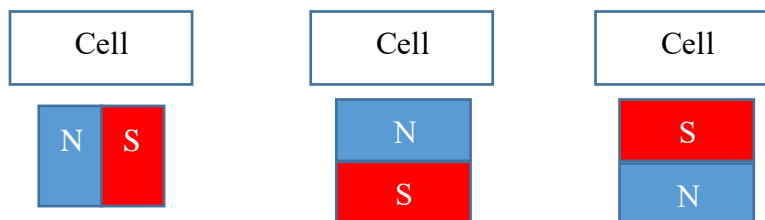
Figure 3-5 The direction of magnetization as Parallel (left), North/N (mid), and South/S (right).

The distribution of ΔG_{ADS} is shown in Figure 3-6 The distribution of L-cys ΔG_{ADS} under different magnetization direction
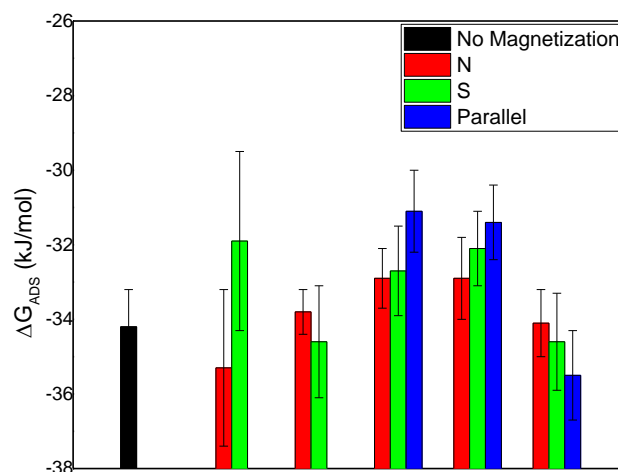
Figure 3-6 The distribution of L-cys ΔG_{ADS} under different magnetization direction. The error bars are the errors listed in Table 3-2 The isotherm calculation results for L-cys adsorption under magnetic field with different directions.

The results above did not show a well-defined trend. A trend would be expected in the ΔG_{ADS} values in which the values for one magnetic field direction should be larger than the other. In some of the data pairs (N/S) above, we observed a larger ΔG_{ADS} values when north pole of the magnetic field is pointing UP than when south is pointing UP, whereas in other cases the opposite is true. It is concluded that the difference in adsorption of chiral molecules is not caused by a thermodynamic effect.

3.2 Chronoamperometry Studies of Cysteine Adsorption/Desorption in Magnetic Fields

3.2.1 Chronoamperometry of Cysteine Adsorption/Desorption

To understand the kinetics of cysteine adsorption/desorption, the mass change on the quartz crystal versus as a function of time was monitored. By applying an electrochemical method, namely chronoamperometry, we could observe the kinetic behaviors between stepwise adsorption and desorption cycles.

In chronoamperometry, or controlled-potential chronoamperometry, the potential applied on the working electrode is stepped. Recalling the oxidative adsorption and reductive desorption, we can apply the anodic peak potential (or more positive) as the higher potential for cysteine adsorption and the cathodic peak potential (or more negative) as the lower potential for desorption stepwise, as shown in Figure 2-1 and Figure 2-3. Applying QCM to measure the frequency change of the quartz crystal during chronoamperometry measurement would give us information about mass change related to adsorption/desorption of cysteine versus time for kinetic studies.

Initially, we considered analyzing the differential of collected mass versus time plot. Considering the general half-reaction equation of cysteine adsorption and desorption:

$$M + RSH = M(I)\text{-}SR + e^- + H^+$$

$$M\text{-}SR + e^- = M + RS^-$$
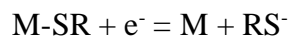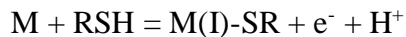
Since the mass change is proportional to the concentrations of unoccupied and occupied binding sites, [M] and [M-SR] on the gold substrate, according to Langmuir model, the mass change rate of the quartz crystal reflects the generating/consuming rate of the M and M-SR species. Considering plotting ln(rate of mass change) versus ln[M] or ln[M-SR] and in practical ln(mass change) we would be able to find out the reaction rate order or adsorption and desorption.

Additionally, for adsorption we are assuming that [RSH], the concentration of cysteine in solution remains unchanged since the overall mass change (several ngs) for cysteine adsorption is negligible compared to the total amount of cysteine within the solution. (While in fact the local concentration of cysteine around the working electrode could be diffusion controlled when the overall concentration of cysteine is relatively slow). In practice, however, the noise level of frequency change versus time data collection was high ($\sim$ 0.2 Hz least versus $\sim$ 3 to 5 Hz of adsorption/desorption caused frequency change), and it caused the differentiation method to not generate useful results.

So eventually a rough assumption was applied that both the adsorption and desorption of cysteine were 1st order reaction (adsorption was actually pseudo-1st order reaction, according to the discussion above). By fitting directly the adsorption frequency versus time data to an exponential decay:

$$y = A_1 e^{(\frac{-x}{t_1})} + y_0$$

And desorption data to an exponential growth:

$$y = A_1 e^{(\frac{x}{t_1})} + y_0$$

As shown in Figure 3-7, the 1st order reaction rate constant k, was calculated as

$$k = \frac{1}{|t_1|}$$

for both adsorption and desorption.
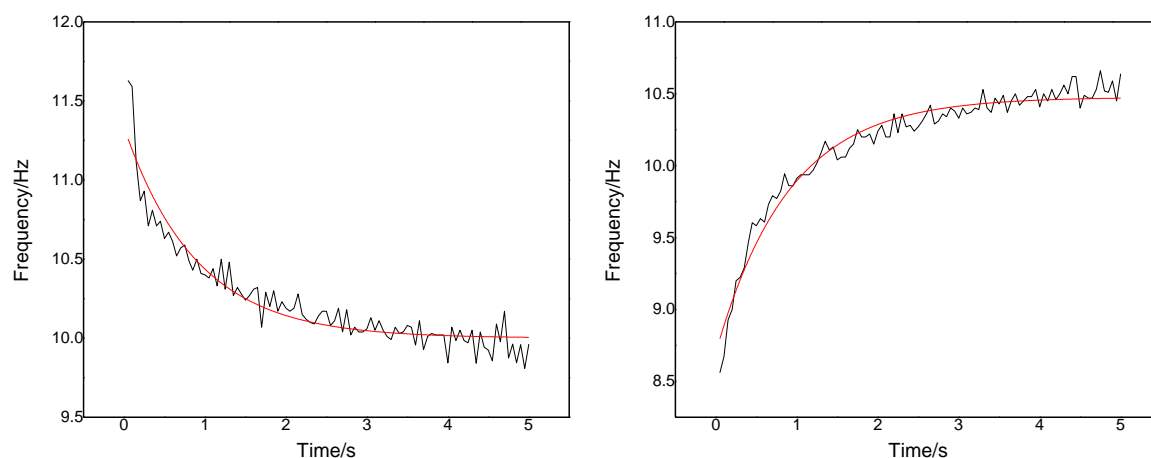
Figure 3-7 Left: fitting cysteine adsorption step in chronoamperometry to exponential decay; right: fitting cysteine desorption step to exponential growth.

3.2.2 Distribution of Adsorption/Desorption Rate Constant in Magnetic Fields

In order to find out whether the CISS effect is influencing the adsorption/desorption rate for different enantiomers of cysteine under different magnetization directions, chronoamperometry measurement of L-cys and D-cys aqueous solution with different concentrations, under parallel, North or South magnetization (as shown in Figure 3-5) was measured. By comparing the rate constants under North magnetization and South magnetization, k_N and k_S, we calculated spin polarization by:

$$P = \frac{k_N - k_S}{k_N + k_S}$$

An example of chronoamperometry measurement of 3μg/mL L-cys solution dissolved in 0.1M pH = 8 potassium phosphate buffer solution under different magnetization directions results

is shown in Figure 3-8. A drift in overall frequency behavior was present in some data part, and it is affecting the values of rate constants got from fitting.
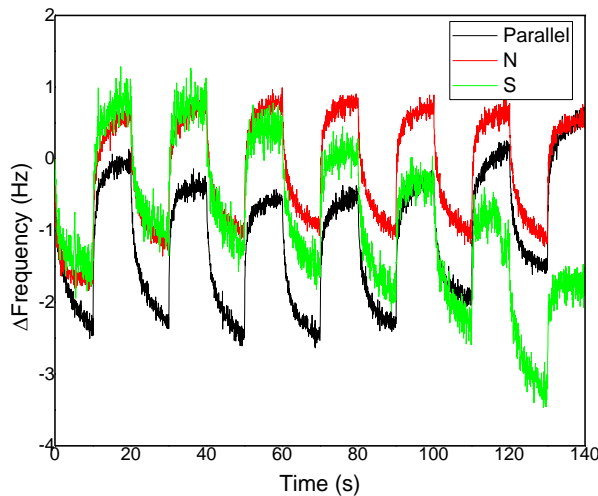
Figure 3-8 Chronoamperometry of 3μg/mL L-cys solution dissolved in 0.1M pH = 8 potassium phosphate buffer solution under different magnetization directions. Electrochemical conditions: Low potential -0.9V vs Ag/AgCl, high potential -0.5V vs Ag/AgCl. Step number =14, step width = 10s. A drift in overall frequency behavior was present in some data part, and it is affecting the values of rate constants got from fitting.

By fitting all of the steps above to exponential rate laws (except for the first adsorption and desorption step because of possible remaining cysteine on gold before experiment) as described in Figure 3-7 and averaging the rate constant values for different L-cys solution concentrations and under different magnetization directions, we were able to list the rate constant values as shown in Table 3-3.

Table 3-3 The rate constant of L-cys adsorption and desorption (1st order)

	k value (1st order)	
	Adsorption*	Desorption*

Concentration of L-cys/µg·mL-1	Parallel	N	S	Parallel	N	S
0.5						
0.75				2.416	1.973	1.383
1				2.947	2.091	1.780
1.25				2.423	2.423	2.234
1.5				1.900	2.583	2.154
1.75				2.032	2.399	2.154
2	0.774	1.161	1.328	2.068	2.347	2.097
2.25	1.632	1.751	1.335	1.664	2.613	3.080
2.5	0.555	2.967	2.526	2.513	1.435	1.234
3	1.602	1.672	1.851	2.373	2.507	2.162
5	1.625	1.896	1.681	3.907	3.042	2.874
10	1.634	1.741	1.895	5.589	3.862	3.251

* The blank area without data values are runs that are unable to fit, mostly due to high noise level.

The rate constant of adsorption does not give a clear trend for N and S. However, for most of desorption k_N is larger than k_S except for the highlighted group, which means that the spin polarization for L-cys desorption is mostly positive. Interestingly, for D-cys the opposite dependence was observed. A plot of polarization for the desorption kinetics with magnetic field is shown in Figure 3-9 A plot of polarization of the desorption kinetics with magnetic field for L-cys (black) and D-cys (red)..
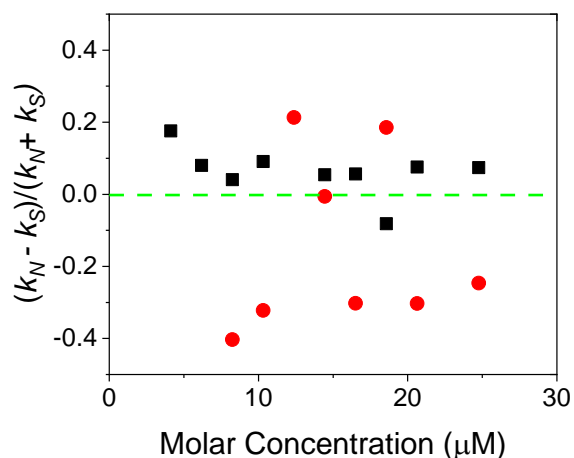
Figure 3-9 A plot of polarization of the desorption kinetics with magnetic field for L-cys (black) and D-cys (red).

Chronoamperometry studies were continued by increasing the step number to 300+ and built up distribution histograms for both the adsorption and desorption. Figure 3-10 shows example histograms of L-cysteine rate constant distribution and corresponding Gaussian fittings used to calculate the average adsorption and desorption rate.
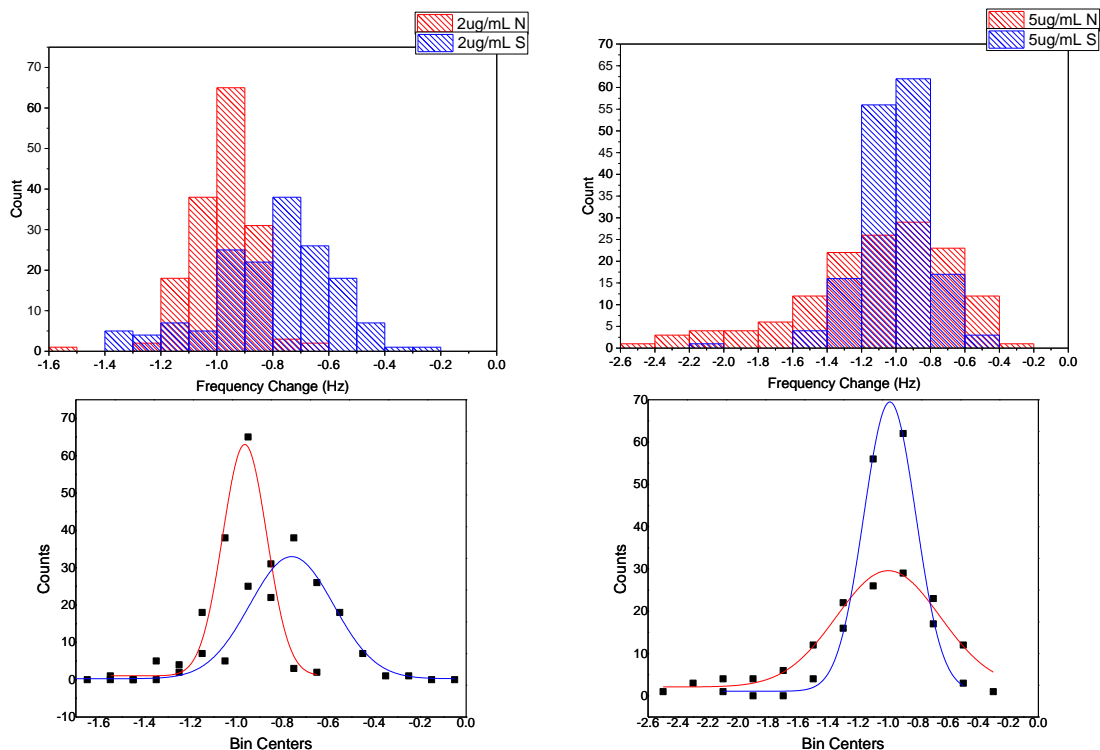
Figure 3-10 Rate constant distribution histogram for 2μg/mL (left) and 5μg/mL (right) L-cysteine adsorption under North (red) or South (Blue) magnetization. The fit line below is the Gaussian fit of the histogram. The average value of rate constant is calculated by the center of Gaussian fit.

A summary chart of L-cysteine and D-cysteine adsorption/desorption rate constant and spin polarization calculation is shown in Table 3-4. A graph showing the distribution of spin polarization is shown as Figure 3-11 The distribution of spin polarization

Table 3-4 A summary chart of L-cys and D-cys adsorption/desorption rate constant and spin polarization

L-cys	Ads			Des		
	k_N	k_S	Spin Polarization	k_N	k_S	Spin Polarization
1μg/mL	0.964	0.484	0.331	1.384	1.285	0.037

	Ads			Des		
2μg/mL	0.964	0.760	0.118			
3μg/mL	1.252	1.171	0.033	5.318	5.580	0.024
5μg/mL	0.999	0.989	0.005	1.226	1.375	0.057
50μg/mL	10.834	7.900	0.157	21.383	23.722	0.052
D-cys	Ads			Des		
	k_N	k_S	Spin Polarization	k_N	k_S	Spin Polarization
1μg/mL	0.302	0.365	-0.094	4.202	4.228	-0.003
2μg/mL	0.353	0.486	-0.159	4.096	4.268	-0.021
3μg/mL	1.080	1.092	-0.006	4.076	3.960	0.014
50μg/mL	8.370	6.365	0.136	11.781	12.622	-0.034

Figure 3-11 The distribution of spin polarization.

37

The result turned out to be different from the conclusions from 7-cycle chronoamperometry in that more of an effect is seen for adsorption than for desorption. For L-cys adsorption, k_N is larger than k_S which makes the spin polarization value positive, and it is the opposite for D-cys. Bo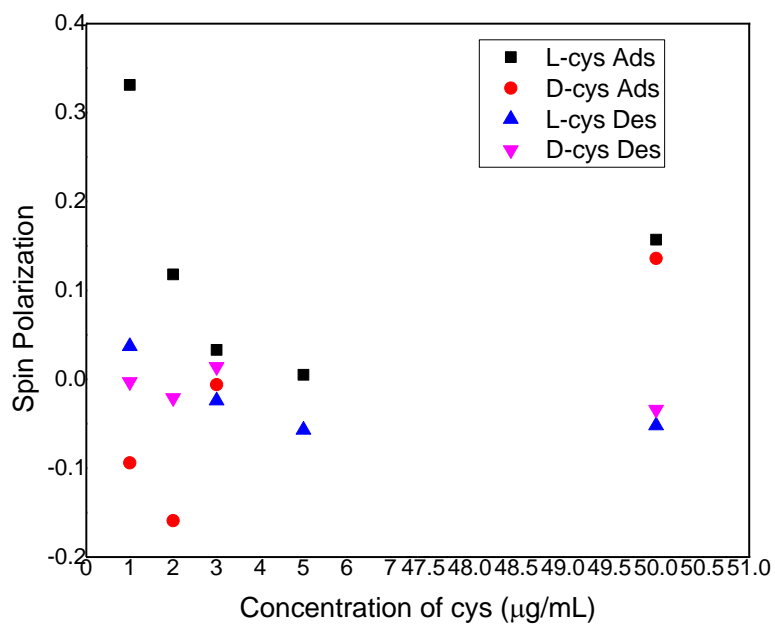th L-cys and D-cys spin polarization for adsorption values has a trend to decrease as the concentration of them goes up. For desorption however, there is not a defined trend for spin polarization sign for either L-cys or D-cys, and spin polarization values are smaller than 6%.

To understand the results, a glance back to our isotherm results and consider the diffusion control of adsorption is needed. According to Figure 3-12 An adsorption isotherm of D-cysteine. The right figure is zoomed in from left from 0 to 0.01mg/mL scale. the concentration selection scale from 1 to 5 μg/mL lies in the kink area of the isotherm, i.e. the transition from unsaturated adsorption to saturation. Recall that the local concentration of cysteine around the working electrode during oxidative adsorption is controlled by diffusion at lower overall cysteine concentrations. As a result, when the concentration of cysteine is low (~1μg/mL), the CISS effect on the interaction between chiral cysteine enantiomers and the ferromagnetic substrate is significant comparing to the low overall reaction rate. When it comes to a higher concentration and closer to saturation, the adsorption rate increases, and diffusion is no longer significant in affecting the rate. The CISS effect on the cys-substrate interaction is thus less significant and the results show a relatively low spin polarization value. The desorption kinetics of cysteine is affected less by cysteine concentration because the diffusion of cysteine is not important for desorption.
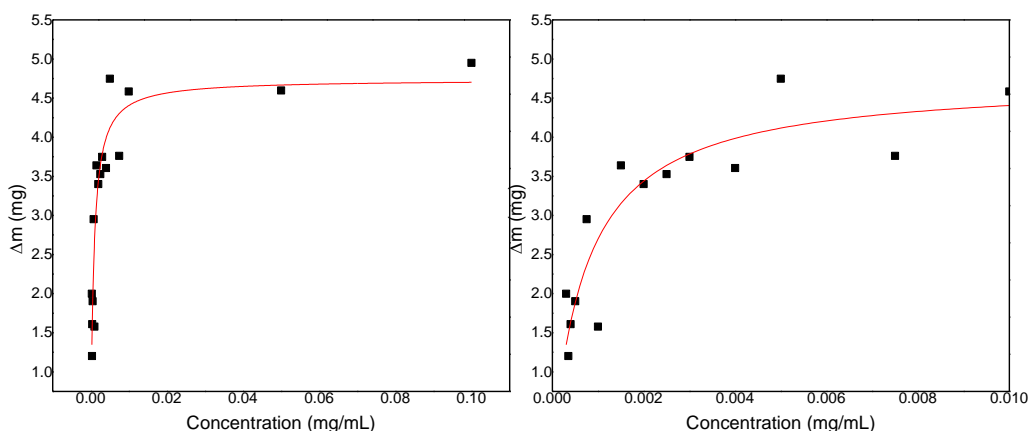
Figure 3-12 An adsorption isotherm of D-cysteine. The right figure is zoomed in from left from 0 to 0.01mg/mL scale.

At 50μg/mL of concentration, however, the spin polarization value increases for adsorption of L-cys and D-cys, though being a highly saturated concentration for adsorption. The underlying reason for this change is not well understood yet.

3.2.3 The Affecting Factors for Chronoamperometry Measurements

Some factors affecting the chronoamperometry measurements are discussed or analyzed below.

Step width. Consider the local concentration around working electrode during adsorption and desorption. When the potential jumps from adsorption to desorption, the release of cysteine from the substrate increases the local concentration of cysteine and makes it temporarily higher than overall concentration. If the step width is too short and adsorption restarts before the mass of cysteine molecules around can diffuse into solution, the high local concentration level will cause error in determining the adsorption rate constant. The chronoamperometry results using the same

solution but different step width is compared. The results are shown in Table 3-5. Comparing the results for 20s adsorption versus that of 5s and 10s, the rate of adsorption is slightly decreased, and it affects the spin polarization value by ~2%. There is not significant improvement to the measurement by varying step width.

Table 3-5 The effect of different step width on spin polarization for 3µg/mL D-cys solution

Step Width	Ads			Des		
	k_N	k_S	Spin Polarization	k_N	k_S	Spin Polarization
5s	1.08	1.092	-0.006	4.076	3.96	0.014
10s	1.08	1.145	-0.029	3.584	3.17	0.061
20s	1.057	1.114	-0.026	2.981	2.893	0.015

pH of the solution. As discussed in 3.1.2, the pH environment of the solution affects the form of cysteine existing in solution and thus the adsorption amount, and possibly also its kinetic behavior in chronoamperometry measurements. The effect of pH environment is shown in Table 3-6 The effect of different pH on spin polarization for 2µg/mL L-cys solution. Strangely for adsorption spin polarization all changed to negative sign for pH = 10, 11 and 12 comparing to 8. The elimination of zwitterion may change the dipole moment within L-cysteine and cause the CISS effect of L-cys to be inverted. On the other hand, as pH increases the desorption rate is lowered and spin polarization increases. This may occur because as the solution becomes more basic there is less tendency to protonate thiolate. This could cause the binding between thiolate and gold substrate to be strengthened and thus the rate of desorption decreases. When the overall rate decreases, the contribution of CISS effect in the difference of k_N and k_S would be more significant, thus increasing the spin polarization value.

Table 3-6 The effect of different pH on spin polarization for 2µg/mL L-cys solution

pH	Ads			Des		
	k_N	k_S	Spin Polarization	k_N	k_S	Spin Polarization
8	0.964	0.760	0.118			
10	0.531	0.609	-0.068	2.650	2.363	0.057
11	0.728	0.772	-0.029	2.170	1.853	0.079
12	0.742	0.813	-0.046	2.194	1.665	0.137

Sample interval. In order to get more detailed information, especially during the sudden change in frequency versus time within the first few ms of each adsorption/desorption step, a low sample interval should be selected for more precise data collection. However, in practice the noise level is going to increase with smaller sample intervals. There is a balance needed between the precision of data collection and signal-to-noise level. The work is to be further explored in the future.

4   Conclusions and Future Directions

In this study, we examined the interaction between cysteine and ferromagnetic substrates, both in thermodynamics and kinetics, as a function of its chirality and the magnetization direction of the ferromagnetic substrate.

In our thermodynamic studies, we investigated how the Gibbs free energy calculated by the Langmuir adsorption model changes with magnetization direction for the same enantiomer of cysteine. Although the measured ΔG_{ADS} values varied somewhat, no discernible trend with magnetization direction or enantiomer could be discerned. It is concluded that the interaction difference is not caused by a thermodynamic effect, but instead a kinetic effect.

In our kinetic studies, it was assumed that the adsorption and desorption of cysteine was a 1st order reaction and chronoamperometry was applied to measure the reaction rate constant under magnetization and then to calculate a spin polarization. The different enantiomers of cysteine showed an opposite sign in trends of k_N and k_S difference and spin polarization. It was also found that the relation between the saturation concentration and spin polarization values, that is, the less overall reaction rate was, the more significant effect of CISS would be on the spin polarization. Some exception and problems were still unsolved though, and it is still needed to improve the overall measuring conditions to ensure a more accurate and precise data collection for better conclusions. If these initial results can be improved upon and made clearer, they may prove useful to guide a further technique to kinetically separate enantiomers of cysteine.

Applying a flow cell in our EQCM system for the thermodynamic studies could be a good improvement. By changing the concentration of the L-cys solution flowing above our substrate sequentially, we may be able to measure different adsorption/desorption data within the same

experimental program and gain enough data for both isotherm and chronoamperometry with more efficiency and better reproducibility. Our future studies with cysteine would be done with EQCM flow cell to hopefully get better results.

References

1.Ray, K.; Ananthavel, S. P.; Waldeck, D. H.; Naaman, R., Asymmetric Scattering of Polarized Electrons by Organized Organic Films of Chiral Molecules. *Science* **1999,** *283* (5403), 814-816.

2.Naaman, R.; Waldeck, D. H., Chiral-Induced Spin Selectivity Effect. *Journal of Physical Chemistry Letters* **2012,** *3* (16), 2178-2187.

3.Naaman, R.; Waldeck, D. H., Spintronics and Chirality: Spin Selectivity in Electron Transport Through Chiral Molecules. *Annual Review of Physical Chemistry* **2015,** *66* (1), 263-281.

4.Baibich, M. N.; Broto, J. M.; Fert, A.; Van Dau, F. N.; Petroff, F.; Etienne, P.; Creuzet, G.; Friederich, A.; Chazelas, J., Giant Magnetoresistance of (001)Fe/(001)Cr Magnetic Superlattices. *Physical Review Letters* **1988,** *61* (21), 2472-2475.

5.Binasch, G.; Grünberg, P.; Saurenbach, F.; Zinn, W., Enhanced Magnetoresistance in Layered Magnetic Structures with Antiferromagnetic Interlayer Exchange. *Physical Review B* **1989,** *39* (7), 4828-4830.

6.Datta, S.; Das, B., Electronic Analog of the Electro-Optic Modulator. **1990,** *56* (7), 665-667.

7.Lu, J. P.; Yau, J. B.; Shukla, S. P.; Shayegan, M.; Wissinger, L.; Rössler, U.; Winkler, R., Tunable Spin-Splitting and Spin-Resolved Ballistic Transport in GaAs/AlGaAs Two-Dimensional Holes. *Physical Review Letters* **1998,** *81* (6), 1282-1285.

8.Dresselhaus, G., Spin-Orbit Coupling Effects in Zinc Blende Structures. *Physical Review* **1955,** *100* (2), 580-586.

9.Rashba, E. I., Properties of Semiconductors with an Extremum Loop. 1. Cyclotron and Combinational Resonance in a Magnetic Field Perpendicular to the Plane of the Loop. *Sov. Phys. Solid State* **1960,** *2*, 1109.

10.Winkler, R., *Spin-Orbit Coupling Effects in Two-Dimensional Electron and Hole Systems*. Springer: 2003; Vol. 191.

11.Gao, X.; Bai, S.; Fazzi, D.; Niehaus, T.; Barbatti, M.; Thiel, W., Evaluation of Spin-Orbit Couplings with Linear-Response Time-Dependent Density Functional Methods. *Journal of Chemical Theory and Computation* **2017,** *13* (2), 515-524.

12.Xie, Z.; Markus, T. Z.; Cohen, S. R.; Vager, Z.; Gutierrez, R.; Naaman, R., Spin Specific Electron Conduction through DNA Oligomers. *Nano Letters* **2011,** *11* (11), 4652-4655.

13. Göhler, B.; Hamelbeck, V.; Markus, T. Z.; Kettner, M.; Hanne, G. F.; Vager, Z.; Naaman, R.; Zacharias, H., Spin Selectivity in Electron Transmission Through Self-Assembled Monolayers of Double-Stranded DNA. *Science* **2011,** *331* (6019), 894-897.

14. Ben Dor, O.; Morali, N.; Yochelis, S.; Baczewski, L. T.; Paltiel, Y., Local Light-Induced Magnetization Using Nanodots and Chiral Molecules. *Nano Letters* **2014,** *14* (11), 6042-6049.

15. Mondal, P. C.; Fontanesi, C.; Waldeck, D. H.; Naaman, R., Spin-Dependent Transport through Chiral Molecules Studied by Spin-Dependent Electrochemistry. *Accounts of Chemical Research* **2016,** *49* (11), 2560-2568.

16. Ravi, S.; Sowmiya, P.; Karthikeyan, A., Magnetoresistance and Spin-Riltering Efficiency of DNA-Sandwiched Rerromagnetic Nanostructures. **2013,** *03* (01), 1350003.

17. Gotesman, G.; Guliamov, R.; Naaman, R., Horizontal versus Vertical Charge and Energy Transfer in Hybrid Assemblies of Semiconductor Nanoparticles. *Beilstein Journal of Nanotechnology* **2012,** *3*, 629-636.

18. Vericat, C.; Vela, M. E.; Benitez, G.; Carro, P.; Salvarezza, R. C., Self-assembled Monolayers of Thiols and Dithiols on Gold: New Challenges for a Well-Known System. *Chemical Society Reviews* **2010,** *39* (5), 1805-1834.

19. Kakiuchi, T.; Usui, H.; Hobara, D.; Yamamoto, M., Voltammetric Properties of the Reductive Desorption of Alkanethiol Self-Assembled Monolayers from a Metal Surface. *Langmuir* **2002,** *18* (13), 5231-5238.

20. Fernanda Carvalhal, R.; Mendes, R.; Kubota, L., *SAM Effects on Riboflavin: A Biomimetic Catalyst for Glucose Oxidation*. 2007; Vol. 2.

21. Matsunaga, M.; Nakanishi, T.; Asahi, T.; Osaka, T., Effect of Surface Coverage of Gold(111) Electrode with Cysteine on the Chiral Discrimination of DOPA. *Chirality* **2007,** *19* (4), 295-299.

22. Walczak, M. M.; Popenoe, D. D.; Deinhammer, R. S.; Lamp, B. D.; Chung, C.; Porter, M. D., Reductive Desorption of Alkanethiolate Monolayers at Gold: a Measure of Surface Coverage. *Langmuir* **1991,** *7* (11), 2687-2693.

23. Possari, R.; Carvalhal, R. F.; Mendes, R. K.; Kubota, L. T., Electrochemical Detection of Cysteine in a Flow System Based on Reductive Desorption of Thiols from Gold. *Analytica Chimica Acta* **2006,** *575* (2), 172-179.

24. Arihara, K.; Ariga, T.; Takashima, N.; Arihara, K.; Okajima, T.; Kitamura, F.; Tokuda, K.; Ohsaka, T., Multiple Voltammetric Waves for Reductive Desorption of Cysteine and 4-Mercaptobenzoic Acid Monolayers Self-Assembled on Gold Substrates. *Physical Chemistry Chemical Physics* **2003,** *5* (17), 3758-3761.

25. Langmuir, I., The Adsorption of Gases on Plane Surfaces of Glass, Mica and Platinum. *Journal of the American Chemical Society* **1918,** *40* (9), 1361-1403.

26. Swenson, H.; Stadie, N. P., Langmuir's Theory of Adsorption: A Centennial Review. *Langmuir* **2019,** *35* (16), 5409-5426.

27. Masel, R., *Principles of Adsorption and Reaction on Solid Surfaces*. Wiley Interscience: 1996.

28. King, W. H., Piezoelectric Sorption Detector. *Analytical Chemistry* **1964,** *36* (9), 1735-1739.

29. Sauerbrey, G. J. Z. f. P., Verwendung von Schwingquarzen zur Wägung dünner Schichten und zur Mikrowägung. **1959,** *155* (2), 206-222.

30. Lorenz, H.; Seidel-Morgenstern, A., Processes To Separate Enantiomers. *Angewandte Chemie International Edition* **2014,** *53* (5), 1218-1250.

31. Stinson, S. C., Chiral Chemistry. *Chemical & Engineering News Archive* **2001,** *79* (20), 45-57.

32. Porter, W. H., Resolution of Chiral Drugs. In *Pure and Applied Chemistry*, 1991; Vol. 63, p 1119.

33. Flack, H., Louis Pasteur's Discovery of Molecular Chirality and Spontaneous Resolution in 1848, Together with a Complete Review of His Crystallographic and Chemical Work. *Acta Crystallographica Section A* **2009,** *65* (5), 371-389.

34. Collet, A., Resolution of Racemates: Did You Say "Classical"? **1998,** *37* (23), 3239-3241.

35. Buhse, T.; Kondepudi, D. K.; Hoskins, B., Kinetics of Chiral Resolution in Stirred Crystallization of D/L-Glutamic Acid. **1999,** *11* (4), 343-348.

36. Schurig, V., Separation of Enantiomers by Gas Chromatography. *Journal of Chromatography A* **2001,** *906* (1), 275-299.

37. Banerjee-Ghosh, K.; Ben Dor, O.; Tassinari, F.; Capua, E.; Yochelis, S.; Capua, A.; Yang, S.-H.; Parkin, S. S. P.; Sarkar, S.; Kronik, L.; Baczewski, L. T.; Naaman, R.; Paltiel, Y., Separation of Enantiomers by Their Enantiospecific Interaction with Achiral Magnetic Substrates. *Science* **2018,** *360* (6395), 1331-1334.

38. Kumar, A.; Capua, E.; Kesharwani, M. K.; Martin, J. M. L.; Sitbon, E.; Waldeck, D. H.; Naaman, R., Chirality-Induced Spin Polarization Places Symmetry Constraints on Biomolecular Interactions. *Proceedings of the National Academy of Sciences of the United States of America* **2017,** *114* (10), 2474-2478.

39. Hamelin, A., Underpotential Deposition of Lead on Single Crystal Faces of Gold: Part I. The Influence of Crystallographic Orientation of the Substrate. *Journal of Electroanalytical Chemistry and Interfacial Electrochemistry* **1984,** *165* (1), 167-180.

40. Heyrovska, R., Precise Molecular Structures of Cysteine, Cystine, Hydrogen-Bonded Dicysteine, Cysteine Dipeptide, Glutathione and Acetyl Cysteine Based on Additivity of Atomic Radii. *Nature Precedings* **2011**.

41. O'Neil, M. J., *The Merck Index - An Encyclopedia of Chemicals, Drugs, and Biologicals*. Royal Society of Chemistry: Cambridge, UK, 2013.

42. Yang, W.; Justin Gooding, J.; Brynn Hibbert, D., Characterisation of Gold Electrodes Modified with Self-Assembled Monolayers of L-Cysteine for the Adsorptive Stripping Analysis of Copper. *J Electroanal Chem* **2001,** *516* (1), 10-16.